HHS Public Access

Author manuscript

Nanoscale. Author manuscript; available in PMC 2024 August 25.

Published in final edited form as:

Nanoscale. ; 15(33): 13595–13602. doi:10.1039/d3nr01801f.

Biodegradable nanoemulsion-based bioorthogonal nanocatalysts for intracellular generation of anticancer therapeutics

Ahmed Nabawy[†],

Aarohi Gupta[†],

Mingdi Jiang,

Cristina-Maria Hirschbiegel,

Stefano Fedeli,

Aritra Nath Chattopadhyay,

Jungmi Park,

Xianzhi Zhang,

Liang Liu,

Vincent M Rotello[*]

Department of Chemistry, University of Massachusetts Amherst, 710 North Pleasant Street, Amherst, Massachusetts 01003, United States

Abstract

Bioorthogonal catalysis mediated by transition metal catalysts (TMCs) provides controlled *in situ* activation of prodrugs through chemical reactions that do not interfere with cellular bioprocesses. The direct use of 'naked' TMCs in biological environments can have issues of solubility, deactivation, and toxicity. Here, we demonstrate the design and application of a biodegradable nanoemulsion-based scaffold stabilized by a cationic polymer that encapsulates a palladium-based TMC, generating bioorthogonal nanocatalyst "polyzymes". These nanocatalysts enhance the stability and catalytic activity of the TMCs while maintaining excellent mammalian cell biocompatibility. The therapeutic potential of these nanocatalysts was demonstrated through efficient activation of a non-toxic prodrug into an active chemotherapeutic drug, leading to efficient killing of cancer cells.

Graphical Abstract

[*]Correspondence: rotello@chem.umass.edu.

[†]Both authors contributed equally

Author contributions

A. Nabawy and A. Gupta contributed equally towards the conceptualization, investigation, and data analysis of the work and the writing of the original draft. M. Jiang, C-M. Hirschbiegel, S. Fedeli, A. N. Chattopadhyay, J. Park, X. Zhang and L. Liu supported the investigation and data analysis of the work. V. M. Rotello helped with the supervision of the work and led the review and editing of the draft.

Conflicts of interest

There are no conflicts to declare.

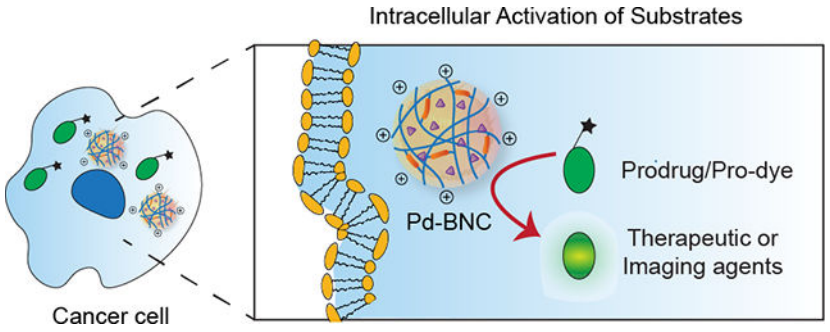

Keywords

Bioorthogonal chemistry; nanoemulsion; intracellular catalysis; prodrug; anticancer

Introduction

Bioorthogonal catalysis using transition metal catalysts (TMCs) has emerged as a versatile tool for biomedical applications, employing catalytic reactions that do not occur naturally in living systems.[1–2,3,4] Uncaging reactions catalyzed by TMCs allow *in situ* generation of therapeutic agents with high specificity and efficiency while minimizing off-target toxicity.[5–6,7,8,9.] In this strategy, drug caging is utilized to restrict prodrug activity until the masking group is removed to generate the active drug within the target cells.[10–11,12,13] Prodrugs are particularly promising for the treatment of tumors as they provide a pathway to avoid adverse effects associated with current chemotherapy.[14–15,16] TMC-based prodrug activation, especially in cancer therapy, enables localized drug generation with enhanced cytotoxic effects.[4,17,18] 'Naked' bioorthogonal TMCs face multiple challenges, including poor aqueous solubility and limited stability in biological environments.[19]

Encapsulation of TMCs into robust delivery platforms enhances the solubility and stability of the catalysts by protecting TMCs from deactivation and retaining their catalytic properties in complex biological media.[20–21,22,23] Inorganic nanomaterials have been used for encapsulating TMCs, generating stable bioorthogonal 'nanozymes' with high catalytic efficiency.[19,24] These nanozymes provide *in situ* 'drug nanofactories' for several therapeutic applications, including cancer and infectious diseases.[25–26,27] However, inorganic nanomaterials are typically non-degradable and can persist within the body, causing unwanted side effects.[28–29,30,31,32]

Polymers have emerged as effective platforms for bioorthogonal TMC encapsulation and delivery,[33] featuring high biocompatibility,[34,35] facile modularity,[36] and scalability.[37] Recent studies have shown that polymeric nanoparticles loaded with TMCs, such as palladium catalysts, had low acute toxicity and provided efficient anticancer therapy through tumor accumulation and activation of anticancer prodrugs.[38,39] More recently, TMCs encapsulated within cationic polymers provide efficient bioorthogonal nanocatalysts that follow the Michaelis–Menten kinetic model (polyzymes) for anticancer and antimicrobial therapeutics.[40,41] Engineering the polymer structure can improve the encapsulation efficiency and hence the catalytic activity of polyzymes.[42–43,44] Functional groups on

polymers can then control cellular uptake and targeting properties of polyzymes.[45,46] Finally, polymeric scaffolds can be engineered with degradable moieties to reduce toxic effects due to the long-term accumulation of non-degradable counterparts.[32,47–48,49,50,51]

We report here the fabrication of biodegradable nanoemulsion-based nanocatalysts (**Pd-BNC**) for the intracellular activation of anticancer prodrugs. The oil-in-water nanoemulsion consists of a carvacrol (oregano oil) oil phase that solubilizes the hydrophobic palladium-based TMC and an amphiphilic poly(oxanorborneneimide) (PONI)-based polymeric scaffold that forms a dynamically crosslinked nanoassembly.[52] Loading palladium-based TMCs into nanoemulsions provides an efficient and biocompatible catalytic platform for therapeutic applications owing to the use of non-toxic polymers and natural essential oil-based components. These polyzymes demonstrated minimal mammalian cell toxicity and hemolytic activity and were readily degraded in the presence of endogenous biomolecules such as glutathione and esterases. **Pd-BNC** efficiently entered and accumulated inside the cells *via* endocytosis, as shown by the uncaging of pro-fluorophores. The potential therapeutic application of **Pd-BNC** was highlighted through *in situ* activation of a doxorubicin prodrug, providing efficient killing of cancer cells. Overall, the modularity, catalytic efficiency, and biodegradability of **Pd-BNC** present a promising strategy for *in situ* generation of imaging and therapeutic agents.

Results and discussions

Generation and characterization of nanocatalysts.

The **Pd-BNC** nanocatalysts were generated by encapsulation of Pd-based TMC into the essential oil core of a biodegradable nanoemulsion (BNE). Carvacrol, a major component of oregano oil, provides the oil phase of the nanoemulsion and serves to solubilize the TMCs. The aqueous phase contains an amphiphilic poly(oxanorborneneimide) (PONI) polymeric scaffold that features three functionalities- guanidinium, maleimide, and tetra(ethylene glycol) monomethyl ether moieties (TEG) ((Figure 1a). The cationic guanidinium moieties impart water solubility and allow interaction with the negatively charged cell membrane, facilitating the endocytic uptake of the nanocatalysts.[53–54,55,56] The TEG moieties enhance the scaffold amphiphilicity allowing the assembly of the polymer and carvacrol into an emulsion. Finally, the maleimide moiety serves to stabilize the nanoemulsions *via* crosslinking with dithiol-disulfide (DTDS), containing disulfide bonds, solubilized inside the carvacrol oil. The crosslinking strategy employs a maleimide-thiol Michael addition reaction to provide degradability. This dynamically crosslinked polymer contains multiple biodegradable points, including 1) disulfides that are degradable through disulfide exchange with endogenous glutathione (GSH) and 2) ester moieties that are cleavable through esterase activity.44 (Degradable points are highlighted in Figure 1b).

The hydrophobic palladium (Pd) catalyst, (1,1′-bis(diphenylphosphino) ferrocene) palladium (II) dichloride, was incorporated into the carvacrol oil phase of the nanoemulsion. This catalyst was chosen as Pd-based systems have shown highly efficient, specific bioorthogonal depropargylation reactions of chemotherapeutic drugs in living cells[57,58–59] and *in vivo*.[37,38] Notably, compared to conventional TMC loading methodologies, our nanoemulsion-based strategy involves an organic solvent-free encapsulation of the Pd-

catalyst into the oil core without further washing steps. This solvent-free approach is particularly advantageous since using organic solvent presents a purification challenge and can result in the loss of encapsulated materials during and after fabrication.

Pd-BNC was generated by emulsification of carvacrol suspension loaded with DTDS (3 wt%) and Pd catalyst (3 mg/mL) with aqueous PONI-GMT (6 μM, 54kDa MW) solution (Figure 1b). We loaded the nanoemulsions with the maximum amount of Pd catalysts based on the catalyst solubility in carvacrol oil (~ 3mg/mL of carvacrol oil), with the nanoemulsion formulation based on our previous studies.[49,50,52]. The final formulation of the polyzyme: Pd catalyst: DTDS crosslinker: carvacrol oil: PONI-GMT polymer of 0.06:0.6:18:1 (weight ratio), with Upon emulsification, PONI-GMT and carvacrol self-assemble and form stable emulsion-based nanocatalysts. The **Pd-BNC** had a diameter of ~300 nm as determined by dynamic light scattering (DLS) with a low polydispersity index (PDI = 0.06) (Figure 2a). This size range is also considered appropriate for *in vivo* use.[60,61] TEM micrographs revealed that **Pd-BNC** adopts a spherical morphology with a size range similar to DLS measurements (Figure 2b). We also confirmed the spherical morphology of **Pd-BNC** using confocal microscopy imaging of larger micron-sized analogs of **Pd-BNC**. Cyanine-5 (Cy5, red fluorescence) was conjugated to PONI-GMT polymers, while 3,3-dioctadecyloxacarbocyanine (DiO, green fluorescence) was loaded within the oil, and we used confocal microscopy to visualize these emulsions. Both green and red fluorescence were co-localized across the particles, indicating a nanoemulsion morphology (Figure S1). The zeta potential measurements of **Pd-BNC** demonstrated a positive surface charge (+35 mV) due to the presence of guanidinium groups (Figure 2c). The amount of palladium catalyst loaded in the **Pd-BNC** was quantified using inductively coupled plasma mass spectrometry (ICP-MS, Figure S2) with ~0.05 mg Pd catalyst per mg polymer. The encapsulation efficiency of the Pd catalyst within the nanoemulsions was calculated as ~80% by comparing the catalyst feed ratio to the actual Pd loading (by ICP-MS). ICP-MS of Pd-BNC before and after 3 washes with phosphate-buffered saline (PBS) was compared and showed that Pd loading is affected negligibly, ensuring minimal Pd leakage. Moreover, elemental mapping analysis was done using energy-dispersive X-ray spectroscopy (EDX), which confirmed the presence and encapsulation of the Pd catalyst within the nanoemulsions (Figure S3). **Pd-BNC** and its components, carvacrol oil, and PONI-GMT polymers, were also characterized by FT-IR spectroscopy, which shows presence of both polymer and oil within the Pd-BNC (Figure S4 and S5).

Catalysis of Pd-BNC in solution.

The catalytic efficacy of **Pd-BNC** nanocatalysts in solution was assessed by bioorthogonal uncaging of N-propargyl-caged Rhodamine 110 (**Pro-Rho**) (Figure 3a). An increase in fluorescence was observed due to the production of fluorescent Rhodamine (**Rho**) after the addition of **Pd-BNC** (60 nM polymer, 220 nM of Pd catalyst) to **Pro-Rho** (2 μM) in PBS at 37 °C, with no significant change in the fluorescence of **Pro-Rho** only (Figure 3b). The catalytic activity of **Pd-BNC** before and after crosslinking was also compared (Figure S6a), showing **Pd-BNC** is active in both non-crosslinked and crosslinked states. Also, free catalyst dispersed in carvacrol oil was completely inactive when compared to **Pd-BNC**, showing crosslinked polymer-based nanoemulsion helps in stabilizing and solubilizing

TMCs (Figure S6b). Interestingly, at high concentrations of **Pro-Rho** substrate, these nanocatalysts displayed a substrate inhibition catalytic behavior (Figure 3c and S7).[62] Such a catalytic model is observed when the velocity of the reaction decreases with an increase in substrate concentration, a common phenomenon in several natural enzymes,[48,63,64] where high concentrations of the substrate can produce allosteric attenuation in catalysis. The maximum reaction rate (V_{max} = 3.1 μM/min) and Michaelis constant (K_m = 1.9 M) were calculated using the Michaelis-Menten equation with substrate inhibition using GraphPad Prism 5 (Figure S7c).

Degradability and biocompatibility of Pd-BNC.

The degradability of the **Pd-BNC** nanocatalysts was explored in the presence of glutathione (GSH) and ester-hydrolyzing enzyme porcine liver esterase (PLE) *via* monitoring changes in particle size through DLS. **Pd-BNC** was incubated with physiologically relevant concentrations of GSH (10 mM) and PLE (35 μM) for 24 h and compared to **Pd-BNC** in PBS as a control. DLS analysis revealed that **Pd-BNC** maintained their stability in PBS even after 24 h (Figure 4a). However, a significant increase in **Pd-BNC** size was observed in either GSH or PLE solutions, indicating the degradation of these nanocatalyst emulsions in the presence of endogenous biomolecules followed by aggregation of oil droplets through different mechanisms including Ostwald ripening.[65,66] We also observed decreased stability of **Pd-BNC**, as noticed by the increase in the nanocatalyst size, when fabricated in the absence of the DTDS crosslinker (Figure S8).

Acute toxicity is a critical consideration for clinical applications of nanocatalysts. The cytotoxicity of **Pd-BNC** was first tested against non-cancerous mammalian fibroblast cells. Different concentrations of **Pd-BNC** were incubated with NIH-3T3 mouse fibroblasts for 24 h, and the cell viability was quantified by Alamar Blue assay. Figure 4b shows that **Pd-BNC** demonstrated no toxicity at therapeutically relevant concentrations. We also evaluated the mammalian cell toxicity of individual **Pd-BNC** components, including the Pd-loaded carvacrol oil and PONI-GMT polymers, and observed no effect on fibroblast viability (Figure S9). Next, the hemolytic activity of **Pd-BNC** was also tested with human red blood cells for further biocompatibility studies. Similar to the Alamar Blue assay, **Pd-BNC** showed negligible lysis of red blood cells (Figure 4c). Finally, we investigated the ability of **Pd-BNC** to induce an inflammatory response in RAW 264.7 macrophages by monitoring mRNA levels of primary inflammatory mediators, TNF-α and iNOS, using Quantitative Reverse Transcription-Polymerase Chain Reaction (qRT-PCR). As shown in Figure 4d, levels of TNF-α and iNOS mRNA expression in **Pd-BNC**-treated macrophages were similar to untreated cells, indicating no apparent inflammatory response from the nanocatalysts.

Intracellular bioorthogonal catalysis in cancer cells.

After validating the catalytic properties of **Pd-BNC** in solution, we next explored their intracellular activity and localization in HeLa cells using confocal microscopy studies. First, PONI-GMT was tagged with Cyanine-5 (Cy5), a red fluorescent dye, to allow tracking of the nanocatalyst. Next, **Pd-BNC** (60 nM polymer, 220 nM of Pd catalyst) was incubated with HeLa cells for 24 h to allow cellular uptake. The cells were then washed three times with PBS to remove excess or surface-attached nanocatalysts. As shown in Figure 5, HeLa

cells exhibited punctate red fluorescence consistent with endosomal localization. The uptake of Pd-BNC by an endosomal process[67] was verified using Lysotracker Blue that co-localized with Cy5-labelled nanocatalysts (Figure S10).

Uncaging was studied by adding fresh media containing **Pro-Rho** (50 μM) to the cells, followed by incubation for 6 h. Bright green fluorescence from uncaging of rhodamine co-localized with the red fluorescence of the polymer scaffold, indicating catalytic uncaging of the pro-dye mediated by the nanocatalysts. Cells incubated with **Pro-Rho** only showed minimal green fluorescence, highlighting the bioorthogonality of this catalytic approach.

Activation of an anticancer prodrug using the nanocatalysts.

We next evaluated the therapeutic potential of **Pd-BNC** through uncaging of an anticancer prodrug. The DNA-targeting chemotherapeutic drug doxorubicin (**Dox**) was chosen owing to its high efficacy against several cancer types.[68] Amine functionalization of **Dox** with propargyl carbamate was used to block its activity and provide a non-toxic prodrug (**Pro-Dox**).[69] Catalytic activation of **Pro-Dox** through **Pd-BNC** releases the active chemotherapeutic agent leading to cancer cell death (Figure 6a). For *in vitro* studies, HeLa cells were first incubated with **Pd-BNC** for 24 h, then washed with PBS to remove any non-internalized nanocatalyst. Cells were then incubated with different concentrations of **Pro-Dox** for another 24 h. Cells treated with either **Pro-Dox** only or **Dox** only were used as negative and positive controls, respectively. Toxicity was observed in cells treated with both **Pd-BNC** and **Pro-Dox**, while incubation with the prodrug caused minimal toxicity. (Figure 6b). The observed efficacy was somewhat lower than for free **Dox**, presumably due to lower intracellular levels of uncaged **Dox** generated by **Pd-BNC**. Notably, despite their lipophilic differences, both **Pro-Dox** (clogP = 1.30) and **Pro-Rho** (clogP = 3.76) exhibited effective transformation to free substrates.[70] The Pd-BNC nanocatalyst can therefore be used across substrates with diverse physicochemical properties.

Conclusion

In summary, polymeric nanoemulsions present a modular and biocompatible platform for encapsulation and intracellular delivery of transition metal catalysts with high catalytic efficiency. These nanocatalysts demonstrated excellent stability while degraded in the presence of specific biomolecules, hence avoiding clearance issues of inorganic nanomaterials. The nanocatalysts provided efficient bioorthogonal activation of prodrugs and imaging probes inside cells. The polymer-based nanocatalysts present here offer a promising platform for *in situ* generation of diagnostics and therapeutics and can improve treatment strategies for cancer and other life-threatening diseases. The tunable size range and modular structure of the **Pd-BNC** platform can be used to control biodistribution and potentially target tumors using stimuli-responsive and targeted polyzymes.

Supplementary Material

Refer to Web version on PubMed Central for supplementary material.

Acknowledgements

This research was supported by the National Institutes of Health under R01 EB022641 and R01 AI134770. C.-M.H. was partially supported by a fellowship from the Chemistry-Biology Interface Training Program (National Research Service Award T32 GM139789). The content is solely the responsibility of the authors and does not necessarily represent the official views of the National Institutes of Health. Imaging and EDX data were obtained in the Light Microscopy Facility and Nikon Center of Excellence at the Institute for Applied Life Sciences (IALS), UMass Amherst with support from the Massachusetts Life Sciences Center. ICP-MS data was obtained in the Mass Spectrometry Core Facility at IALS, UMass Amherst.

References

1. Platts K, Michel R, Green E, Gillam T, Ghetia M, O'Brien-Simpson N, Li W, Blencowe C, Blencowe A, Bioconjug. Chem. 2021, 32, 1845–1851. [PubMed: 34254789]
2. Bai Y, Chen J, Zimmerman SC, Chem. Soc. Rev. 2018, 47, 1811–1821. [PubMed: 29367988]
3. Völker T, Meggers E, Curr. Opin. Chem. Biol. 2015, 25, 48–54. [PubMed: 25561021]
4. Weiss JT, Dawson JC, Macleod KG, Rybski W, Fraser C, Torres-Sánchez C, Patton EE, Bradley M, Carragher NO, Unciti-Broceta A, Nat. Commun. 2014, 5, 3277. [PubMed: 24522696]
5. Clavadetscher J, Hoffmann S, Lilienkampf A, Mackay L, Yusop RM, Rider SA, Mullins JJ, Bradley M, Angew. Chemie Int. Ed. 2016, 55, 15662–15666.
6. Streu C, Meggers E, Angew. Chemie - Int. Ed. 2006, 45 (34), 5645–5648.
7. S. R. Thomas, A. Casini, Curr. Opin. Chem. Biol. 2020, 55, 103–110. [PubMed: 32086166]
8. Kaur J, Saxena M, Rishi N, Bioconjug. Chem. 2021, 32, 1455–1471. [PubMed: 34319077]
9. Yusop RM, Unciti-Broceta A, Johansson EMV, Sánchez-Martín RM, Bradley M, Nat. Chem. 2011, 3, 239–243 [PubMed: 21336331]
10. Rooseboom M, Commandeur JNM and Vermeulen NPE, Pharmacol. Rev, 2004, 56, 53–102. [PubMed: 15001663]
11. Dong Y, Tu Y, Wang K, Xu C, Yuan Y and Wang J, Angew. Chemie Int. Ed, 2020, 59, 7168–7172.
12. Robinson MA, Charlton ST, Garnier P, Wang X, Davis SS, Perkins AC, Frier M, Duncan R, Savage TJ, Wyatt DA, Watson SA and Davis BG, Proc. Natl. Acad. Sci, 2004, 101, 14527–14532. [PubMed: 15448212]
13. Sun I-C, Yoon HY, Lim D-K and Kim K, Bioconjug. Chem, 2020, 31, 1012–1024. [PubMed: 32163277]
14. Xie A, Hanif S, Ouyang J, Tang Z, Kong N, Kim NY, Qi B, Patel D, Shi B and Tao W, EBioMedicine, 2020, 56, 102821. [PubMed: 32505922]
15. Giang I, Boland EL and Poon GMK, AAPS J, 2014, 16, 899–913. [PubMed: 25004822]
16. Kavanaugh WM, Expert Opin. Biol. Ther, 2020, 20, 163–171. [PubMed: 31779489]
17. Pérez-López AM, Rubio-Ruiz B, Sebastián V, Hamilton L, Adam C, Bray TL, Irusta S, Brennan PM, Lloyd-Jones GC, Sieger D, Santamaría J and Unciti-Broceta A, Angew. Chemie - Int. Ed., 2017, 56, 12548–12552.
18. Sun T, Lv T, Wu J, Zhu M, Fei Y, Zhu J, Zhang Y and Huang Z, J. Med. Chem, 2020, 63, 13899–13912. [PubMed: 33141588]
19. Zhang X, Huang R, Gopalakrishnan S, Cao-Milán R, Rotello VM, Trends Chem. 2019, 1, 90–98 [PubMed: 34095799]
20. Zhang X, Fedeli S, Gopalakrishnan S, Huang R, Gupta A, Luther DC and Rotello VM, ChemBioChem, 2020, 21, 2759–2763. [PubMed: 32400081]
21. Jeong Y, Tonga GY, Duncan B, Yan B, Das R, Sahub C and Rotello VM, Small, 2018, 14, 1–5.
22. Li C-H, Huang R, Makabenta JM, Schmidt-Malan S, Patel R and Rotello VM, Microbiol. Insights, 2021, 14, 117863612199712.
23. Fedeli S, Im J, Gopalakrishnan S, Elia JL, Gupta A, Kim D and Rotello VM, Chem. Soc. Rev, 2021, 50, 13467–13480. [PubMed: 34787131]
24. van Hest J, Zheng G and Rotello VM, Bioconjug. Chem, 2021, 32, 1409–1410. [PubMed: 34323066]

25. Zhang X, Liu Y, Gopalakrishnan S, Castellanos-Garcia L, Li G, Malassiné M, Uddin I, Huang R, Luther DC, Vachet RW and Rotello VM, ACS Nano, 2020, 14, 4767–4773. [PubMed: 32227914]
26. Hardie J, Makabenta JM, Gupta A, Huang R, Cao-Milán R, Goswami R, Zhang X, Abdulpurkar P, Farkas ME and Rotello VM, Mater. Horizons, 2022, 9, 1489–1494.
27. V Makabenta JM, Nabawy A, Li C-H, Schmidt-Malan S, Patel R, Rotello VM, Nat. Rev. Microbiol. 2021, 19, 23–36 [PubMed: 32814862]
28. Bobo D, Robinson KJ, Islam J, Thurecht KJ and Corrie SR, Pharm. Res, 2016, 33, 2373–2387. [PubMed: 27299311]
29. Zhang X, Lin S, Huang R, Gupta A, Fedeli S, Cao-Milán R, Luther DC, Liu Y, Jiang M, Li G, Rondon B, Wei H and Rotello VM, J. Am. Chem. Soc, 2022, 144, 12893–12900. [PubMed: 35786910]
30. Zhou H, Ge J, Miao Q, Zhu R, Wen L, Zeng J and Gao M, Bioconjug. Chem, 2020, 31, 315–331. [PubMed: 31765561]
31. Roy S, Liu Z, Sun X, Gharib M, Yan H, Huang Y, Megahed S, Schnabel M, Zhu D, Feliu N, Chakraborty I, Sanchez-Cano C, Alkilany AM and Parak WJ, Bioconjug. Chem, 2019, 30, 2751–2762. [PubMed: 31621306]
32. Mohammapdour R and Ghandehari H, Adv. Drug Deliv. Rev, 2022, 180, 114022. [PubMed: 34740764]
33. Nabawy A, Huang R, Luther DC, Zhang X, Li C-H, Makabenta JM and Rotello VM, Chem. Sci, 2022, 13, 12071–12077. [PubMed: 36349111]
34. Guo B, Sheng Z, Hu D, Li A, Xu S, Manghnani PN, Liu C, Guo L, Zheng H and Liu B, ACS Nano, 2017, 11, 10124–10134. [PubMed: 28892609]
35. Oz Y, Nabawy A, Fedeli S, Gupta A, Huang R, Sanyal A and Rotello VM, ACS Appl. Mater. Interfaces, 2021, 13, 40325–40331. [PubMed: 34416106]
36. Cole JP, Lessard JJ, Lyon CK, Tuten BT and Berda EB, Polym. Chem, 2015, 6, 5555–5559.
37. Zhu DY, Landis RF, Li C-H, Gupta A, Wang L-S, Geng Y, Gopalakrishnan S, Guo JW and Rotello VM, Nanoscale, 2018, 10, 18651–18656. [PubMed: 30264837]
38. Miller MA, Askevold B, Mikula H, Kohler RH, Pirovich D and Weissleder R, Nat. Commun, 2017, 8, 15906. [PubMed: 28699627]
39. Miller MA, Mikula H, Luthria G, Li R, Kronister S, Prytyskach M, Kohler RH, Mitchison T and Weissleder R, ACS Nano, 2018, 12, 12814–12826. [PubMed: 30550257]
40. Zhang X, Landis RF, Keshri P, Cao-Milán R, Luther DC, Gopalakrishnan S, Liu Y, Huang R, Li G, Malassiné M, Uddin I, Rondon B and Rotello VM, Adv. Healthc. Mater, 2021, 10, 2001627.
41. Huang R, Li C-H, Cao-Milán R, He LD, Makabenta JM, Zhang X, Yu E and Rotello VM, J. Am. Chem. Soc, 2020, 142, 10723–10729. [PubMed: 32464057]
42. Huerta E, Stals PJM, Meijer EW and Palmans ARA, Angew. Chemie - Int. Ed, 2013, 52, 2906–2910.
43. Liu Y, Pujals S, Stals PJM, Paulöhrl T, Presolski SI, Meijer EW, Albertazzi L and Palmans ARA, J. Am. Chem. Soc, 2018, 140, 3423–3433. [PubMed: 29457449]
44. Bickerton S, Jiwpanich S and Thayumanavan S, Mol. Pharm, 2012, 9, 3569–3578. [PubMed: 23088589]
45. Chen J, Li K, Shon JS and Zimmerman SC, J. Am. Chem. Soc, 2020, 142, 4565–4569. [PubMed: 32100539]
46. Bai Y, Feng X, Xing H, Xu Y, Kim BK, Baig N, Zhou T, Gewirth AA, Lu Y, Oldfield E and Zimmerman SC, J. Am. Chem. Soc, 2016, 138, 11077–11080. [PubMed: 27529791]
47. Li C-H, Landis RF, Makabenta JM, Nabawy A, Tronchet T, Archambault D, Liu Y, Huang R, Golan M, Cui W, Mager J, Gupta A, Schmidt-Malan S, Patel R and Rotello VM, Mater. Horizons, 2021, 8, 1776–1782.
48. Prajapati SK, Jain A, Jain A and Jain S, Eur. Polym. J, 2019, 120, 109191.
49. Nabawy A, Makabenta JM, Schmidt-Malan S, Park J, Li C-H, Huang R, Fedeli S, Chattopadhyay AN, Patel R and Rotello VM, J. Control. Release, 2022, 347, 379–388. [PubMed: 35550914]
50. Nabawy A, Makabenta JM, Li C-H, Park J, Chattopadhyay AN, Schmidt-Malan S, Gupta A, Patel R, Rotello VM, ACS Biomater. Sci. Eng. 2020, 7, 1780–1786. [PubMed: 33966379]

51. Karlsson J, Vaughan HJ and Green JJ, Annu. Rev. Chem. Biomol. Eng, 2018, 9, 105–127. [PubMed: 29579402]
52. Landis RF, Li C-H, Gupta A, Lee Y-W, Yazdani M, Ngernyuang N, Altinbasak I, Mansoor S, Khichi MAS, Sanyal A and Rotello VM, J. Am. Chem. Soc, 2018, 140, 6176–6182. [PubMed: 29709168]
53. Sahay G, Alakhova DY and Kabanov AV, J. Control. Release, 2010, 145, 182–195. [PubMed: 20226220]
54. Basu Roy S, Nabawy A, Chattopadhyay AN, Geng Y, Makabenta JM, Gupta A and Rotello VM, ACS Appl. Mater. Interfaces, 2022, 14, 27515–27522.
55. Azevedo C, Macedo MH and Sarmento B, Drug Discov. Today, 2018, 23, 944–959. [PubMed: 28919437]
56. Harush-Frenkel O, Debotton N, Benita S and Altschuler Y, Biochem. Biophys. Res. Commun, 2007, 353, 26–32. [PubMed: 17184736]
57. Weiss JT, Carragher NO and Unciti-Broceta A, Sci. Rep, 2015, 5, 9329. [PubMed: 25788464]
58. Destito P, Sousa-Castillo A, Couceiro JR, López F, Correa-Duarte MA and Mascareñas JL, Chem. Sci, 2019, 10, 2598–2603. [PubMed: 30996975]
59. Tonga GY, Jeong Y, Duncan B, Mizuhara T, Mout R, Das R, Kim ST, Yeh YC, Yan B, Hou S and Rotello VM, Nat. Chem, 2015, 7, 597–603. [PubMed: 26100809]
60. Wilhelm S, Tavares AJ, Dai Q, Ohta S, Audet J, Dvorak HF and Chan WCW, Nat. Rev. Mater, 2016, 1, 16014.
61. Kang H, Rho S, Stiles WR, Hu S, Baek Y, Hwang DW, Kashiwagi S, Kim MS and Choi HS, Adv. Healthc. Mater, 2020, 9, e1901223. [PubMed: 31794153]
62. Reed MC, Lieb A and Nijhout HF, BioEssays, 2010, 32, 422–429. [PubMed: 20414900]
63. Jones PA and Takai D, Science (80)., 2001, 293, 1068–1070.
64. Winge I, McKinney JA, Ying M, D'Santos CS, Kleppe R, Knappskog PM and Haavik J, Biochem. J, 2008, 410, 195–204. [PubMed: 17973628]
65. Fredrick E, Walstra P and Dewettinck K, Adv. Colloid Interface Sci, 2010, 153, 30–42. [PubMed: 19913777]
66. Solans C, Izquierdo P, Nolla J, Azemar N and Garcia-Celma MJ, Curr. Opin. Colloid Interface Sci, 2005, 10, 102–110.
67. Wexselblatt E, Esko JD and Tor Y, J. Org. Chem, 2014, 79, 6766–6774. [PubMed: 25019333]
68. Thorn CF, Oshiro C, Marsh S, Hernandez-Boussard T, McLeod H, Klein TE and Altman RB, Pharmacogenet. Genomics, 2011, 21, 440–446. [PubMed: 21048526]
69. Wang X, Liu Y, Fan X, Wang J, Ngai WSC, Zhang H, Li J, Zhang G, Lin J and Chen PR, J. Am. Chem. Soc, 2019, 141, 17133–17141. [PubMed: 31580665]
70. Leo AJ, Chem. Rev, 1993, 93, 1281–1306.

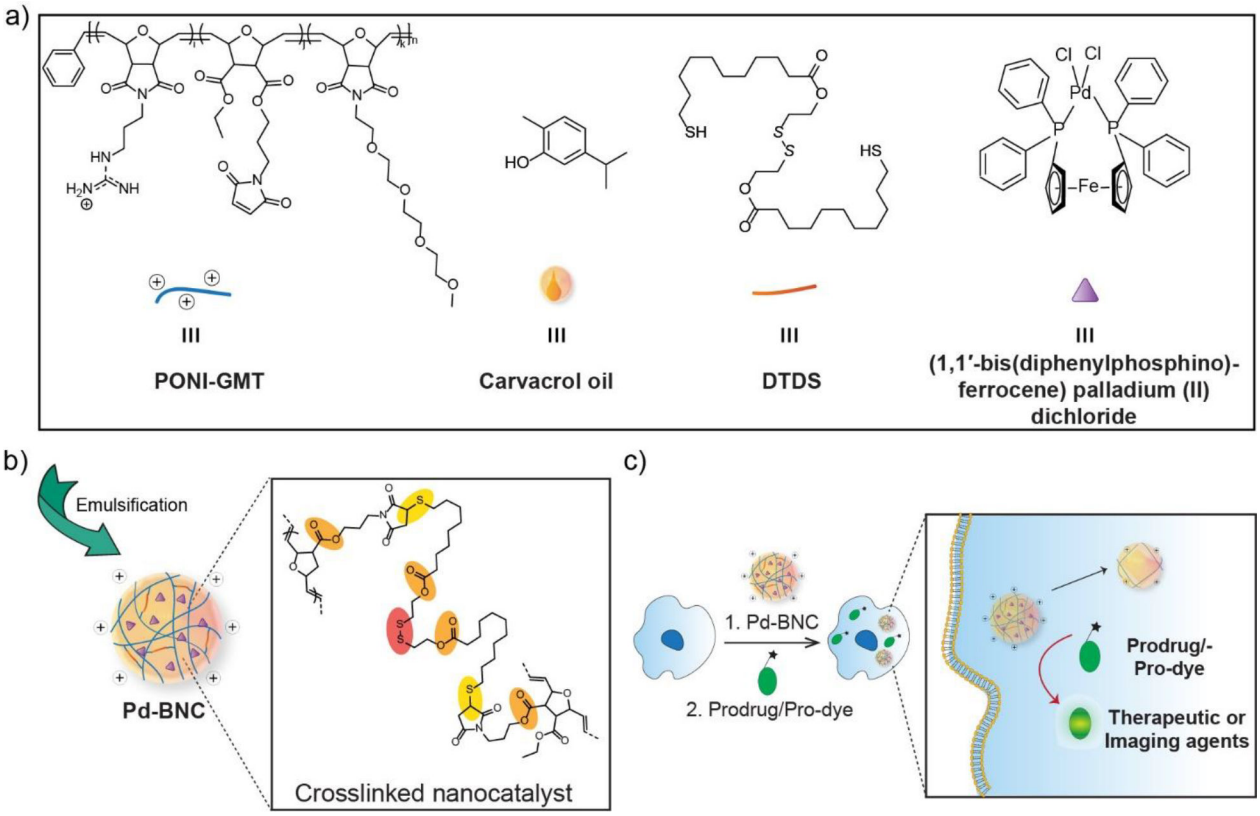

Figure 1.

a) Chemical structures of PONI-GMT, carvacrol oil, DTDS, and Pd-based catalyst. b) Fabrication of **Pd-BNC** from emulsification of aqueous PONI-GMT polymer and Pd-catalyst in carvacrol oil crosslinked with DTDS; biodegradable points are highlighted. Crosslinking imparts stability and biodegradability. c) Schematic of intracellular bioorthogonal activation of substrates *in situ* by **Pd-BNC**.

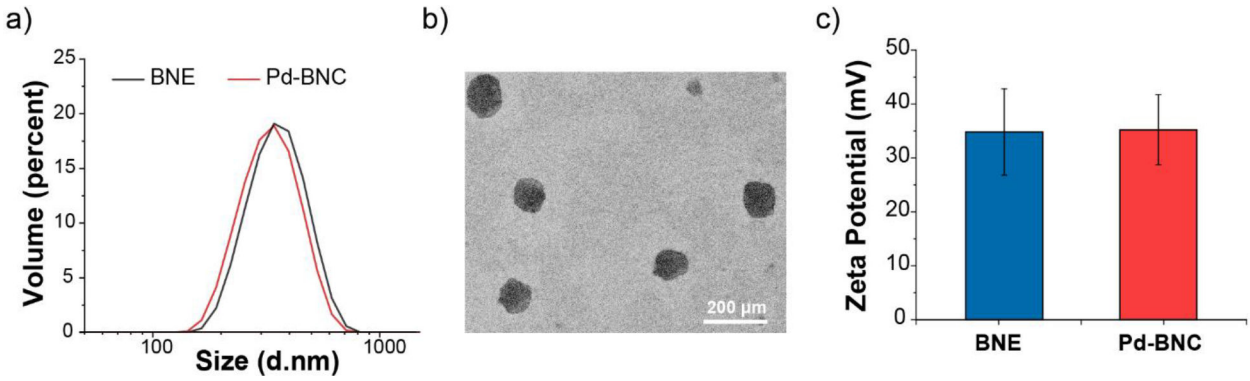

Figure 2.

a) Dynamic light scattering (DLS) histogram of **BNE** and **Pd-BNC** in phosphate-buffered saline (150 mM). b) TEM micrograph of **Pd-BNC**. c) Zeta potential measurement of BNE and **Pd-BNC**. Values are expressed as mean ± standard deviation of ≥3 replicates.

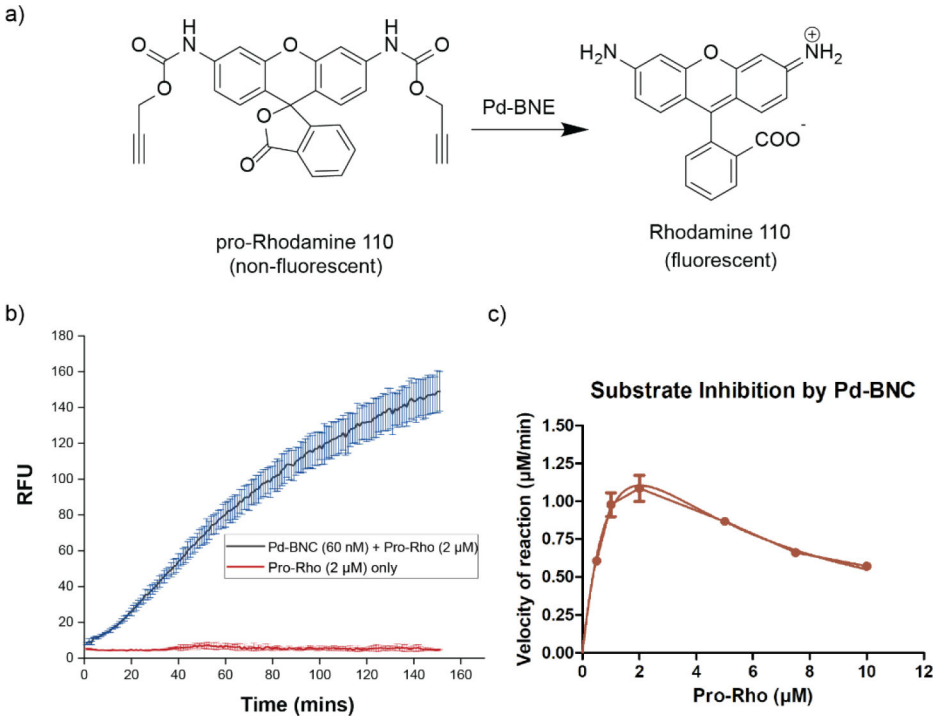

Figure 3.

a) Bioorthogonal depropargylation of Pro-Rhodamine (**Pro-Rho**) to fluorescent Rhodamine by **Pd-BNC** at 37 °C. b) Kinetic study of **Pro-Rho** (2 μM) with **Pd-BNC** (60 nM polymer, 220 nM of Pd catalyst) over time. c) Reaction velocity by **Pd-BNC** as a function of substrate concentration

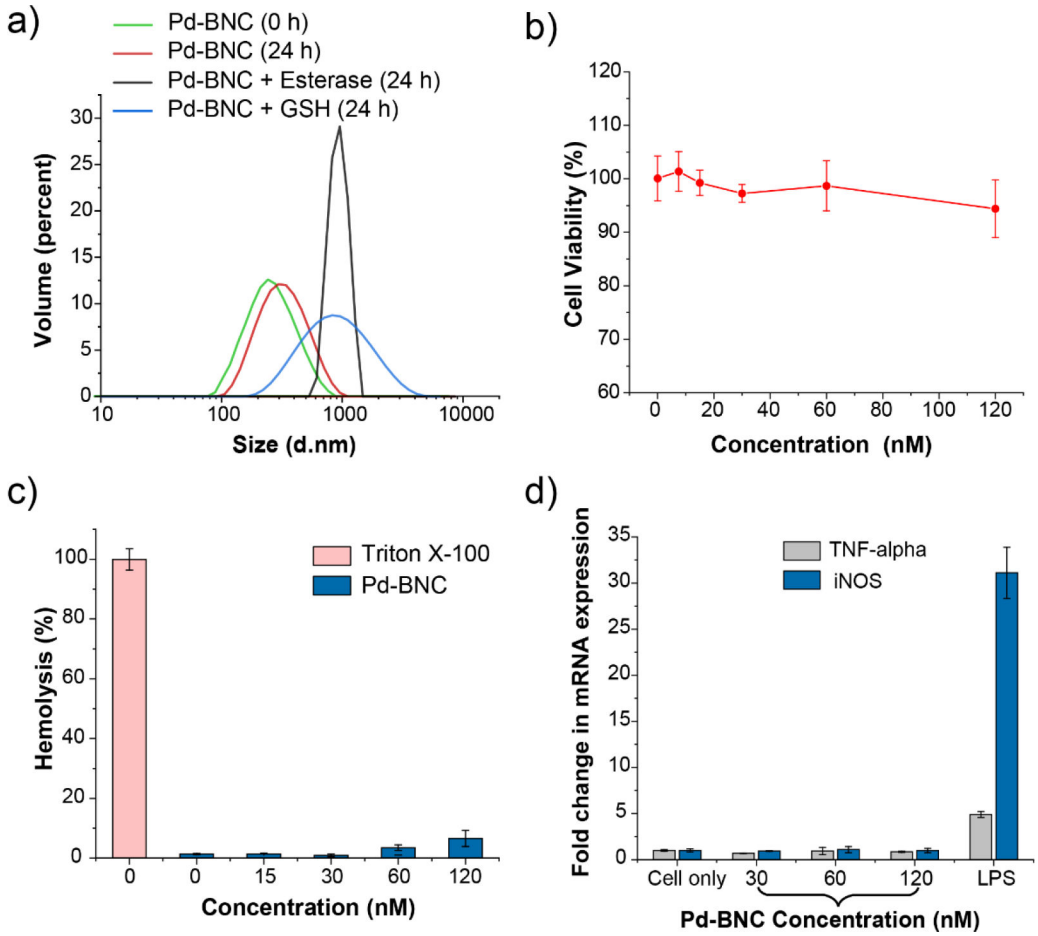

Figure 4.

a) DLS analysis of **Pd-BNC** in the presence of either porcine liver esterase (PLE) and GSH at 37°C. The size of **Pd-BNC** increased due to degradation and subsequent aggregation of oil droplets. b) Viability of human fibroblast NIH-3T3 cells (ATCC CRL-1658) after 24 h exposure to **Pd-BNC**. c) Hemolytic activity of **Pd-BNC** at different concentrations indicates their non-hemolysis. d) mRNA quantification of inflammation markers, TNF-a and iNOS, in RAW 264.7 macrophages. Values are expressed as mean ± standard deviation of ≥3 replicates.

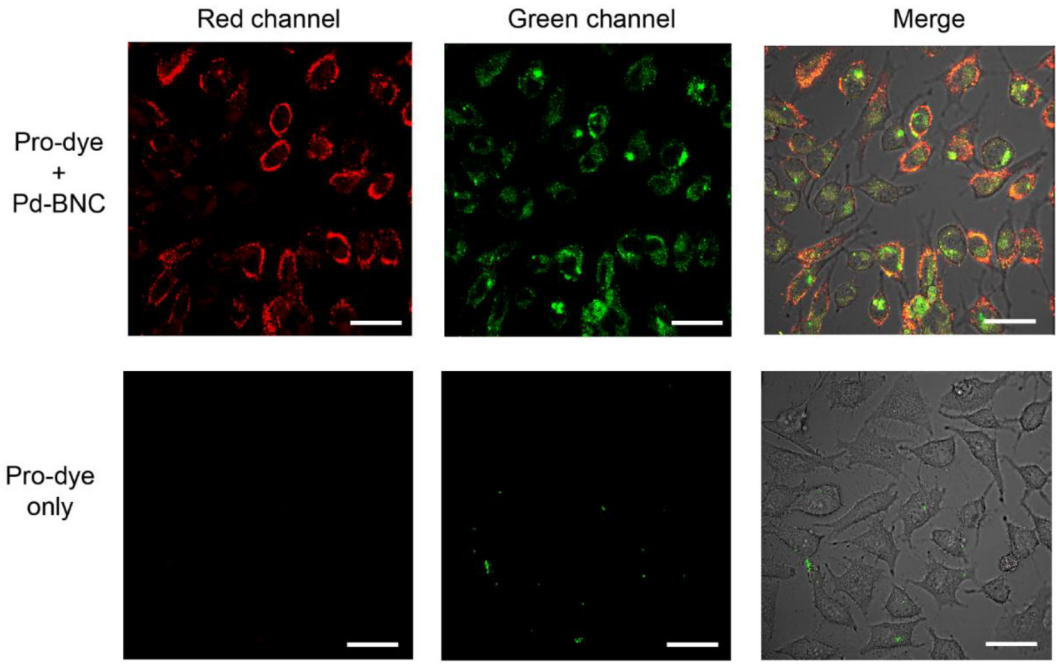

Figure 5.

Confocal images of HeLa cells incubated with or without Cy5-labelled **Pd-BNC** nanocatalysts (24 h, (60 nM polymer, 220 nM of Pd catalyst)), followed by incubation with **Pro-Rho** (50 μM). Cells incubated with **Pro-Rho** only showed no fluorescence inside cells, as expected. Cells treated with Cy5-labelled **Pd-BNC** and **Pro-Rho** showed bright green fluorescence from the activation of **Pro-Rho**. The green fluorescence co-localized with red fluorescence from Cy5-labelled **Pd-BNC**, confirming the activation was due to the catalytic effect of nanocatalysts. (Scale bar = 20 μm).

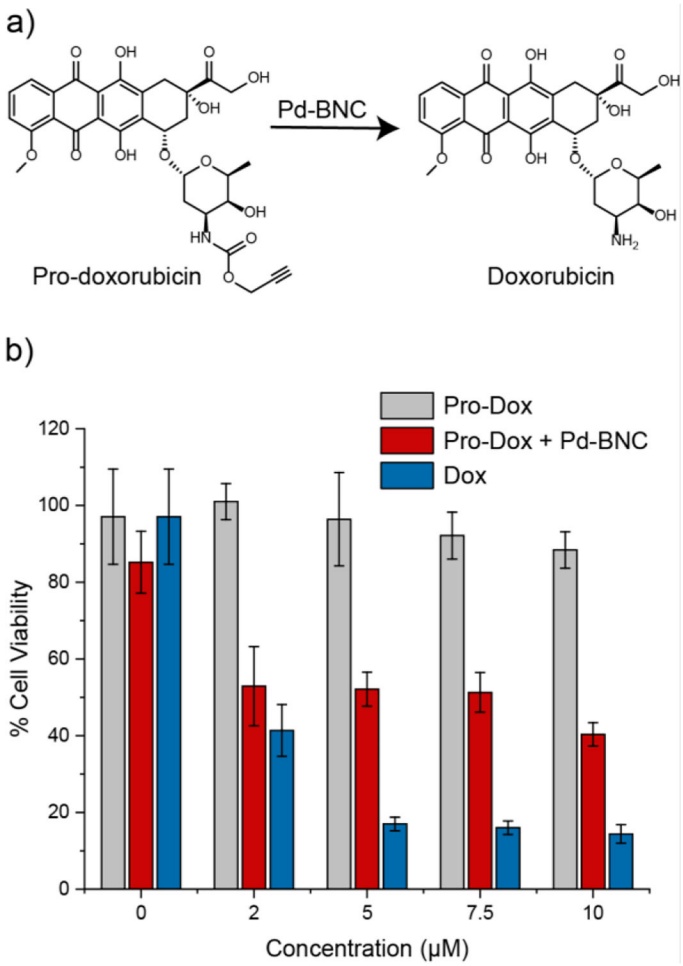

Figure 6.

a) Schematic representation of the activation of Pro-Doxorubicin (**Pro-Dox**) by **Pd-BNC**. b) Cell viability of HeLa cells after **Pro-Dox** activation by **Pd-BNC**